ARCHIVES of FOUNDRY ENGINEERING

ISSN (1897-3310)
Volume 11
Issue 4/2011

13 – 18

3/4

Published quarterly as the organ of the Foundry Commission of the Polish Academy of Sciences

Cellular automaton modeling of ductile iron microstructure in the thin wall

A.A. Burbelko*, D. Gurgul, W. Kapturkiewicz, J. Początek, M. Wróbel
Faculty of Foundry Engineering, AGH University of Science and Technology, Reymonta 23, 30-059 Krakow, Poland
*Corresponding author. E-mail address: abur@agh.edu.pl

Received 01.07.2011; accepted in revised form 27.07.2011

Abstract

The mathematical model of the globular eutectic solidification in 2D was designed. Proposed model is based on the Cellular Automaton Finite Differences (CA-FD) calculation method. Model has been used for studies of the primary austenite and of globular eutectic grains growth during the solidification of the ductile iron with different carbon equivalent in the thin wall casting. Model takes into account, among other things, non-uniform temperature distribution in the casting wall cross-section, kinetics of the austenite and graphite grains nucleation, and non-equilibrium nature of the interphase boundary migration. Solidification of the DI with different carbon equivalents was analyzed. Obtained results were compared with the solidification path calculated by CALPHAD method.

Keywords: Cellular Automaton, Modeling, Ductile Iron, Solidification, Microstructure

1. Introduction

Nodular graphite cast iron, also known as ductile iron (DI), has major applications in critical engineering parts due to its mechanical properties and castability. The mechanical and physical properties of this material depend on the chemical composition, shape and number of the graphite grains and microstructure of the metallic matrix.

Solidification of DI was a subject of many computer modeling programs described in literature [1-5], in which the stationary conditions of carbon diffusion in austenite is pre-assumed. Recently, a tendency for production of thin-walled castings has been observed [6-8]. In this technology, the process of the fast solidification is very far from equilibrium and steady-state conditions.

The purpose of the present work is a two-dimension model development for simulation of the DI structure formation during the solidification in the condition of non steady-state temperature and diffusion fields in the thin-wall casting.

2. Model of process

The CA-FD is one of the known methods of the simulation of microstructure formation during the solidification [9, 10]. In the CA microstructure modeling the grain shape during and after solidification is the result of the simulation and does not superimposed beforehand. The model development for a one-phase microstructure evolution is a subject of the numerous researches [11-20]. Model of the eutectic solidification of DI in the uniform temperature field and superimposed cooling rate is known [21].

Presented model is based on the CA-FD technique and will predict solidification of DI in the non-uniform temperature field during the cooling of the thin-wall casting. Model takes into account the continuous nucleation of austenite and graphite grains from liquid controlled by undercooling, separate non-equilibrium growth of graphite nodules and austenite dendrites at the first solidification stage, and the following cooperative growth of graphite-austenite eutectic in the binary Fe-C system.

A set of six cell states for microstructure modeling was used: three mono-phase states – "liquid", "austenite", and "graphite" –

and three two-phase states. At the beginning, all of the cells in the CA lattice are in the "liquid" state and have initial temperature. Nucleation and growth of the solid grains are possible when the temperature of the liquid drops below the liquidus line for proper phase.

2.1. Heat and mass diffusion

The numerical solution of the nonlinear Fourier equation was used for heat flow:

$$c \cdot \partial T/\partial \tau = \nabla \cdot (\lambda \nabla T) + q_T \tag{1}$$

where: T is the temperature, τ is the time, λ is the thermal conductivity, c is the volumetric specific heat, and q_T is the latent heat generation rate.

Solute diffusion was calculated in the same manner as temperature distribution, by the numerical solution of the diffusion equation with a source term at the interface:

$$\partial C/\partial \tau = \nabla \cdot (D \nabla C) + q_C \tag{2}$$

where D is the solute diffusion coefficient, and C is the solute concentration in this phase.

Both source functions are equal to zero outside of the interface cells. In the interface cells the heat and mass sources for the finite-difference scheme are:

$$q_T = L_{\alpha \to \beta} \cdot \partial f_\beta / \partial \tau \tag{3}$$

$$q_C = (C_\alpha - C_\beta) \cdot \partial f_\beta / \partial \tau \tag{4}$$

where $L_{\alpha \to \beta}$ is the volumetric latent heat of $\alpha \to \beta$ transformation, C_α and C_β are the carbon concentration in the vanishing and growing phases, and f_β is the growth of the new phase volume fraction during the time step.

For thermal and diffusion calculation in the computational domain, the following boundary conditions (BC) were used for outer boundary: periodic BC at the top and bottom of the grid; symmetry BC at the left side; at the right side (mold) – an absence of mass flow and heat flow according to Schwarz task:

$$q = b_m (T_b - T_m) / \sqrt{\pi \tau} \tag{5}$$

where b_m is a mold heat accumulation coefficient (for sand mold b_m = 1.04 $W \cdot m^{-2} K^{-1}$), and difference between temperature in the "mold-casting" contact T_b and initial mold temperature T_m is assumed equal to 1000 K.

Eq. (1) was solved in the whole of analyzed domain with the BC described above. Eq. (2) was solved separately in the every continuous domain of every phase bordered by interphase boundary. In addition, the source function (4) was used for the internal BC calculation on the interphase boundaries.

The details of solution are described in [22].

2.2. Nucleation

Grain nucleation in industrial alloys has a heterogeneous nature. The substrates for the nucleus are randomly distributed in the bulk. Bulk distribution of differently-sized substrates also has the random nature. The undercooling value of substrate activation is a function of its size. Functional relationship between the active substrate fraction and undercooling ΔT_n should be a feature of the probability distribution law [23]. The undercooling value of each phase should be calculated relative to the appropriate liquidus lines. The Weibull statistical distribution was used in this paper for nucleation modeling [24]. The specific number of active substrates is given by:

$$n = N_{\max} \exp(-b/\Delta T_n) \tag{6}$$

where $N_{\max}$ and b are the nucleation parameters.

The undercooling of nucleation can be calculated as

$$\Delta T_n = -b / \ln[p/(\upsilon N_{\max})] \tag{7}$$

where υ is a cell's volume (or surface for 2D), and p is a random number generated with an equiprobability distribution in the (0..1] range.

The values for N_{max} and b used in the present work for the modeling of graphite and austenite grains nucleation are listed in the Table 1. The method of continuous nucleation modeling used has been presented in details in the [25]. The solid grain will begin to grow when the undercooling exceeds the above level. The substrates are present (and nucleation will possible) only in the cells with the positive ΔT_n value. The state of the CA cell with the active nucleus varies from "liquid" to "austenite" or "graphite" when the local undercooling exceeds ΔT_n level. The states of adjacent liquid cells are changed to the appropriate interface. The new phase growth and volume fraction change are only possible in the interface cells.

Table 1.
Nucleation parameters.

	Austenite	Graphite
b, K	5	50
N_{max}, m^{-2}	$3.0 \cdot 10^8$	$1.0 \cdot 10^9$

2.3. Grain growth

The kinetic undercooling of the mother liquid phase is a measure of the thermodynamic driving force of the growth of new grains. Total undercooling at the solid-liquid interface, hence the difference between the equilibrium solidification temperature T_{Eq} (determined from the phase equilibrium diagram of carbon concentration obtained during simulation on the transformation front) and the real temperature T_r is equal to the sum of capillary undercooling ΔT_κ and kinetic undercooling ΔT_μ:

$$T_{Eq} - T_r = \Delta T_\kappa + \Delta T_\mu \tag{8}$$

where $\Delta T_\kappa = \kappa\Gamma$, Γ is the Gibbs-Thomson coefficient, and κ is a front curvature.

Basing on [26], it has been assumed in the computations that the interface migration rate is a linear function of the local kinetic undercooling ΔT_μ:

$$u = \mu \Delta T_\mu \tag{9}$$

where μ is the kinetic growth coefficient.

The increment of the new phase volume fraction in the interface cells Δf over one time step $\Delta\tau$ in the square CA cells of size a was calculated using the equation proposed in [27]:

$$\Delta f = u\,\Delta\tau / \left[a(|\cos\theta| + |\sin\theta|)\right] \tag{10}$$

where θ is the angle between the X axis and the normal direction of the grain interface.

If the phase volume fraction in the interface cell increases up to 1, this cell varies its state from interface to appropriate one-phase. Additionally, this cell captures all of the adjacent ones: their states exchange to the appropriate interface.

The normal direction of the grain boundary in the interface cells was determined by the approach of the F-vector [28]. The angle θ between the growth direction (normal to the grain boundary) and the positive X-axis direction was calculated as follows:

$$\theta = \arctan\left(\sum_{i,j} y_{i,j} f_{i,j} \Big/ \sum_{i,j} x_{i,j} f_{i,j} \right) \tag{11}$$

where: $f_{i,j}$ is the volume fraction of the phase in the cell (i,j), and $x_{i,j}$ and $y_{i,j}$ are the relative coordinates of the adjacent cells. The summation in (11) concerning the 20 neighboring cells gives the best results of normal direction estimation [28].

Another details of the used CA-FD model of a two-phase eutectic solidification were introduced elsewhere [29,30].

3. Results of modeling

Computations were carried out on a grid of 200×1000 cells. The side of each cell was 1 μm in length. An initial uniform carbon concentration in the binary Fe-C liquid was assumed. Calculation were performed for hypoeutectic (4.2% of carbon), eutectic (4.25%) and hypereutectic (4.3%) compositions for the initial temperatures: 1209.1°C, 1203.0°C, 1221.9°C respectively. Parameters used in the modeling are shown in the Table 2.

Ductile iron solidification in the thin wall 2 mm width has significant nonequilibrium nature. Comparison of the equilibrium temperature dependence of the austenite and graphite volume fractions with the real solidification path of eutectic DI presented in Fig. 1. Curves 1 and 3 indicate mean value of the graphite and austenite volume fractions as a function of mean temperature in the wall cross section. Curves 2 and 4 were obtained by means the Thermo-Calc® software.

Table 2.
Thermo-physical parameters used in the modeling.

Heat conductivity, W/(m·K):		
– liquid	λ_L	30
– austenite	λ_γ	20
– graphite	λ_{gr}	20
Diffusivity of carbon in, m^2/s:		
– liquid	D_L	$1.25\cdot10^{-9}$
– austenite	D_γ	$5\cdot10^{-10}$
Transition heat, J/m^3:		
– liquid – austenite	$L_{L/\gamma}$	$19.7\cdot10^{8}$
– liquid – graphite	$L_{L/gr}$	$16.2\cdot10^{5}$
– austenite – graphite	$L_{\gamma/gr}$	$8.8\cdot10^{5}$
Specific heat, $J/(m^3\cdot K)$:		
– liquid	$c_{v,L}$	$5.6\cdot10^{6}$
– austenite	$c_{v,\gamma}$	$5.84\cdot10^{6}$
– graphite	$c_{v,gr}$	$1.78\cdot10^{6}$
Gibbs-Thomson coefficient for interface, m·K:		
– austenite – liquid	$\Gamma_{\gamma/L}$	$1.9\cdot10^{-7}$
– graphite – liquid	$\Gamma_{gr/L}$	$7.0\cdot10^{-6}$
– graphite – austenite	$\Gamma_{gr/\gamma}$	$9.45\cdot10^{-6}$
Kinetic coefficient of the interface, m/(s·K):		
– austenite – liquid	$\mu_{\gamma/L}$	10^{-3}
– graphite – liquid	$\mu_{gr/L}$	10^{-8}
– graphite – austenite	$\mu_{gr/\gamma}$	10^{-8}

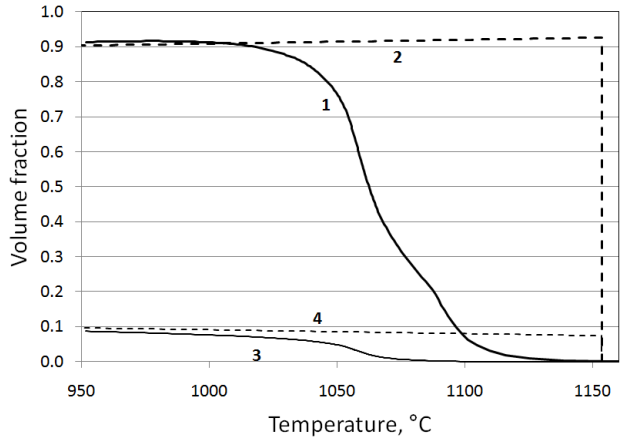

Fig. 1. Austenite (1,2) and graphite (3,4) volume fraction as a function of temperature: 1, 3) CA modeling; 2, 4) thermodynamic equilibrium (obtained by ThermoCalc software)

Cooling curves and cooling rate of the analyzed alloys are presented in Fig. 2 with a kinetic of the austenite and graphite growth. Decreasing of the austenite volume fraction is observed at the end of solidification. This is a result of graphite nodules

growth from the supersaturated austenite. The rate of graphite growth at the end of solidification becomes grater then the austenite solidification rate.

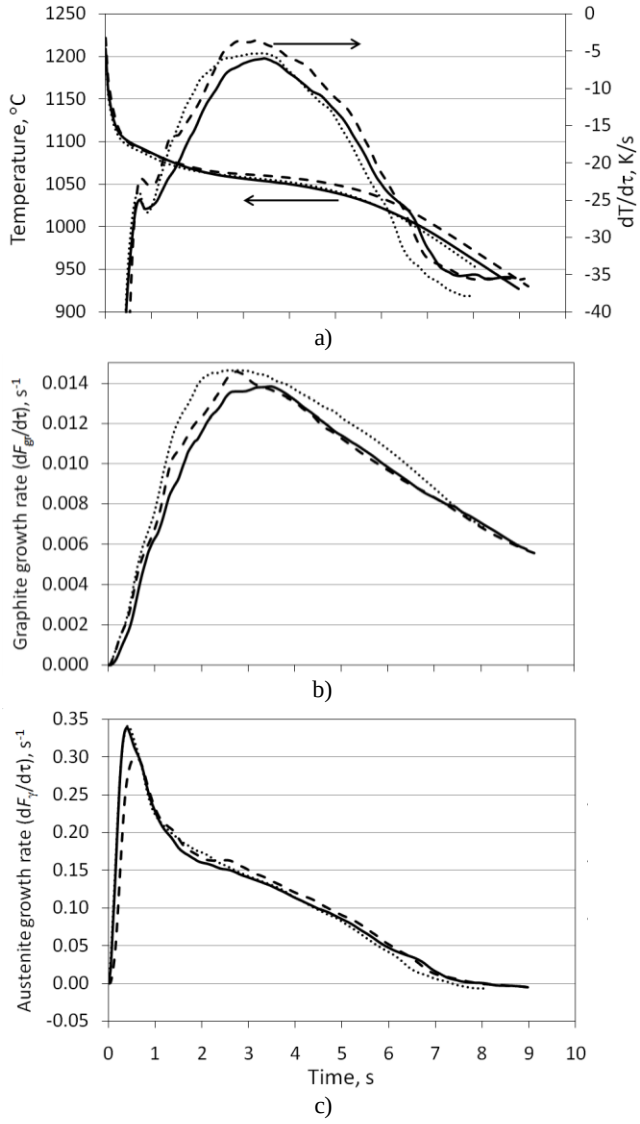

Fig. 2. Cooling curves and cooling rates of DI (a), and graphite (b) and austenite (c) growth rate: solid lines – hypoeutectic DI, dotted lines – eutectic DI, and dashed lines – hypereutectic DI

The history of microstructure formation in the 2 mm casting is presented in Fig. 3. There are no essential differences between solidification of DI with hypo- and hypereutectic composition. Fig. 3 a, d and g present alloy structure in the moment of the highest austenite growth rate. Fig. 3 b, e and h show moment of the highest graphite volume rate. Maximum growth rate of graphite particles volume was observed when all particles of this phase are isolated from liquid by austenite envelope.

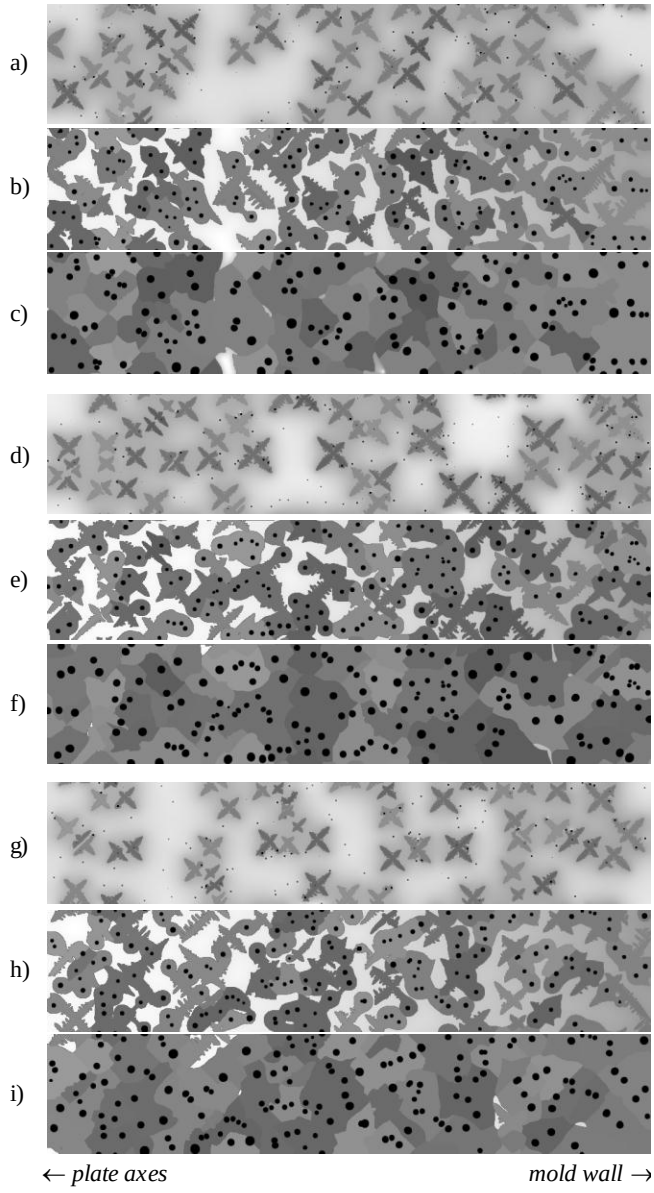

Fig. 3. Structure formation of the hypoeutectic (a-c), eutectic (d-f) and hypereutectic (g-i) DI during the solidification into 2 mm wall (simulation results); solidification time: (a,d,g) – 0.7 s; (b,d,h) – 3.2 s; (c,f,i) – 7.2 s

4. Conclusions

The CAFD computer model for the simulation of the DI solidification in thin walls was presented.

The model is well worked for thin walled ductile iron casting, for the high level undercooling below the equilibrium temperature

and very fast solidification process and makes possible to predict the microstructure changes of the DI during solidification.

Acknowledgements

This work was supported by Polish NCN project No. N N508 621140.

References

[1] D.M. Stefanescu, A. Catalina, X. Guo, L. Chuzhoy, M.A. Pershing and G.L. Biltgen: Prediction of room temperature mcrostructure and mechanical properties in iron castings, MCWASP, edited by B.G. Thomas, C. Beckermann, TMS, Warrendale (1998), p. 455-462.

[2] S.M. Yoo, A. Ludwig and P.R. Sahm: Numerical simulation of solidification of nodular cast iron in permanent molds, in Solidification Processing, edited by J. Beech, H. Jones / Ranmoor House, Univ. of Sheffield (1997), p. 494-497.

[3] S. Chang, D. Shangguan and D. Stefanescu: Modeling of the liquid/solid and the eutectoid phase transformations in spheroidal graphite cast iron, Metal. Trans. A, Vol. 23A (1992), p. 1333-1346.

[4] T. Skaland, O. Grong and T. Grong: A model for the graphite formation in ductile cast iron. II. Solid state transformation reactions, Metal. Trans. A, Vol. 24A (1993), p. 2347-2353.

[5] M. Onsoien, O. Grong, O. Gundersen and T. Skaland: A process model for the microstructure evolution in ductile cast iron. I. The model, Metal. Mat. Trans. A, Vol. 30A (1999), p. 1053-1068.

[6] E. Fraś and M. Górny: Thin wall ductile and austempered iron castings as substitutes for aluminium alloy castings, Foundry Trade Journal Int., Vol. 185, No. 3683 (2011), p. 85-90.

[7] C. Labrecque and M. Gagne: Production of thin-wall ductile iron castings, Int. Journal of Cast Metals Res., Vol. 16 (2003), p. 313-318.

[8] D.M. Stefanescu, R.E. Ruxanda and L.P. Dix: The metllurgy and tensile mechanical properties of thin wall spheroidal graphite irons, Int. Journal of Cast Metals Res., Vol. 16 (2003), p. 319-324.

[9] H. Rafii-Tabar, A. Chirazi: Multiscale computational modelling of solidification phenomena, Physics Reports-Review Section of Phys. Lett., Vol. 365 (2002), p. 145-249.

[10] P.D. Lee, A. Chirazi, R.C. Atwood and W. Wang: Multi-scale modelling of solidification microstructures, including microsegregation and microporosity, in an Al-Si-Cu alloy, Mat. Sci. Eng. A, Vol. 365 (2004), p. 57-65.

[11] A.R. Umantsev, V.V. Vinogradov and V.T. Borisov: Mathematical modeling of the dendrite growth during the solidification from undercooled melt, Kristallografia, Vol. 30 (1985), p. 455-460 (in Russian).

[12] M. Rappaz, Ch.A. Gandin: Probabilistic Modelling of Microstructure Formation in Solidification Processes, Acta Metallurgica et Materialia, Vol. 41 (1993), p. 345-360.

[13] S. Pan, M. Zhu: A three-dimensional sharp interface model for the quantitative simulation of solutal dendritic growth, Acta Materialia, Vol. 58 (2010), p. 340-352.

[14] G. Guillemot, Ch.A. Gandin and M. Bellet: Interaction between single grain solidification and macrosegregation: Application of a cellular automaton-finite element model, Journal of Crystal Growth, Vol. 303 (2007), p. 58-68.

[15] L. Beltran-Sanchez, D.M. Stefanescu: A quantitative dendrite growth model and analysis of stability concepts, Metall. Mat. Trans. A, Vol. 35 (2004), p. 2471-2485.

[16] V. Pavlyk, U. Dilthey: Simulation of weld solidification microstructure and its coupling to the macroscopic heat and fluid flow modelling, Modelling and Simulation in Materials Science and Engineering, Vol. 12 (2004), p. 33-45.

[17] M.F. Zhu, C.P. Hong: A three dimensional modified cellular automaton model for the prediction of solidification micro-structures, ISIJ International, Vol. 42 (2002), p. 520-526.

[18] D.J. Jarvis, S.G.R. Brown and J.A. Spittle: Modelling of non-equilibrium solidification in ternary alloys: comparison of 1D, 2D, and 3D cellular automaton-finite difference simulations, Mat. Sci. Techn., Vol. 16 (2000), p. 1420-1424.

[19] A.A. Burbelko, E. Fraś, W. Kapturkiewicz and D. Gurgul: Modelling of dendritic growth during unidirectional solidification by the method of cellular automata, Mat. Sci. Forum, Vol. 649 (2010), 217-222.

[20] A.A. Burbelko, E. Fraś, W. Kapturkiewicz and E. Olejnik: Nonequilibrium kinetics of phase boundary movement in cellular automaton modelling, Mat. Sci. Forum, Vol. 508 (2006), p. 405-410.

[21] H.L. Zhao, M.F. Zhu, D.M. Stefanescu: Modeling of the divorced eutectic solidification of spheroidal graphite cast iron, Key Eng. Materials, Vol. 457 (2011), p. 324-329.

[22] W. Kapturkiewicz, A.A. Burbelko, E. Fraś, M. Górny, D. Gurugl: Computer modelling of ductile iron solidification using FDM and CA methods, Journal of Achievments in Materials and Manufacturing Engineering, Vol. 43, Iss. 1 (2010), p. 310-323.

[23] Ch.-A. Gandin, M. Rappaz: A coupled finite element-cellular automaton model for the prediction of dendritic grain structures in solidification processes, Acta Metall. Mater., Vol. 42(7) (1994), p. 2233-2246.

[24] E. Fraś, K. Wiencek, A.A. Burbelko, M. Górny: The application of some probability density function of heterogeneous nucleation, Materials Science Forum, Vol. 508, (2006), p. 425-430.

[25] A. Burbelko, E. Fraś, D. Gurgul, W. Kapturkiewicz, J. Sikora: Simulation of the ductile iron solidification using a cellular automaton, Key Engineering Materials, Vol. 457 (2011), p. 330-336.

[26] J. Hoyt, M. Asta: Atomistic computation of liquid diffusivity, solid-liquid interfacial free energy, and kinetic coefficient in Au and Ag, Phys. Rev. B., 65, art. No. 214106 (2002), p. 1–11.

[27] A.A. Burbelko, W. Kapturkiewicz, D. Gurgul: Analysis of causes and means to reduce artificial anisotropy in modelling of the solidification process on cellular automaton, Solidification Processing: Proceedings of the 5th Decennial International Conference on Solidification

Processing. H. Jones eds., The University of Sheffield, UK, 2007, p. 31-35.
[28] U. Dilthley, V. Pavlik: Numerical simulation of dendrite morphology and grain growth with modified cellular automata, Modeling of Casting, Welding and Advanced Solidification Processes VIII, B.G. Thomas and C. Beckermann eds., TMS, Warrendale, 1998, p. 589-596.
[29] A. Burbelko, D. Gurgul: Modeling of primary and eutectic solidification by using CAFD method. in: Computer Methods in Materials Science, Vol. 11, No. 1 (2011), p. 128-134.
[30] D. Gurgul, A.A. Burbelko: Simulation of austenite and graphite growth in ductile iron by means of cellular automata. Archives of Metallurgy and Materials. Vol. 55, Iss. 1 (2010), p. 53-60.